that there yet remains much chemistry to be explored in this area.

Acknowledgment. We are grateful to the National Institute of General Medical Sciences and the National Science Foundation for support of this research. Additional support was provided by the National Institutes of Health (Training Grant CA-09112, R.L.R.), the Deutscher Akademischer Austauschdienst (NATO Science Fellowship, P.P.), and the American Cancer Society (fellowship to W.B.T.). We thank Dr. G. C. Papaefthymiou for assistance in obtaining Mössbauer data at the Francis Bitter National Magnet Laboratory, which was supported by the National Science Foundation, and Dr. P. Nordlund for permission to quote his results prior to publication.

Supplementary Material Available: Tables of atomic coordinates, equivalent isotropic thermal parameters, anisotropic thermal parameters, bond distances and angles, and observed and calculated temperature-dependent magnetic susceptibilities for **1** and **2**, respectively, and the derivation of the temperature-dependent magnetic susceptibility equations for **1** and **2** (79 pages); tables of observed versus calculated structure factors (213 pages). Ordering information is given on any current masthead page.

Steady-State and Time-Resolved Fluorescence Investigations of Pyrene Excimer Formation in Supercritical CO_2†

JoAnn Zagrobelny, Thomas A. Betts, and Frank V. Bright*

Contribution from the Department of Chemistry, Acheson Hall, State University of New York at Buffalo, Buffalo, New York 14214. *Received October 18, 1991. Revised Manuscript Received March 4, 1992*

Abstract: Detailed studies on the formation of pyrene excimer in supercritical CO_2 are reported. The photophysics of pyrene are investigated as a function of temperature and fluid density. Over the broad density range studied, there is no evidence for ground-state (solute–solute) interaction. Comparison is made between excimer formation in supercritical CO_2 and ground-state dimerization of pyrene in γ-cyclodextrin (γ-CD). Time-resolved fluorescence spectrocopy is used to recover the individual rate terms that describe the total emission process. The recovered density-dependent bimolecular rates for pyrene excimer formation in supercritical CO_2 follow a simple diffusion-controlled model. This result parallels reports on pyrene excimer formation in normal liquid solvents. Finally, the relative decrease in pyrene excimer formation, with increased fluid density, is easily explained from our time-resolved experiments.

Introduction

Many physicochemical properties describe a chemical substance or mixture. For example, the boiling point, density, and dielectric constant can all be used to characterize (at least partially) a particular species or system. If a substance is heated and maintained above its critical temperature, it becomes impossible to liquefy it with pressure.[1] Furthermore, when pressure is applied to this system, a single phase forms that exhibits unique physicochemical properties. This single phase is termed a supercritical fluid and is characterized by a critical temperature and pressure (T_c and P_c, respectively).

Supercritical fluids are intriguing and offer a convenient means to adjust a solvent medium from gas- to liquid-like characteristics without actually changing the chemical structure of the medium. Moreover, by proper control of pressure and temperature one can survey a significant range of physicochemical properties (density, diffusivity, viscosity, dielectric constants, etc.) without ever passing through a phase boundary. That is, a supercritical fluid can be considered a continuously adjustable solvent.

As a consequence of their unique characteristics, supercritical fluids have received a great deal of attention in a number of important scientific fields.[1-14] Often there are many reasons given for choosing a supercritical fluid over another medium, but it turns out that that choice is governed typically by the following: (1) the ease with which the chemical potential can be varied simply by adjustment of the system pressure[13] and (2) the unique solvation and favorable mass transport properties.[5]

Over the past decade, much progress is supercritical fluid science and technology has occurred. For example, supercritical fluids have found widespread use in extractions,[2-5] chromatography,[6-9] chemical reaction processes,[10,11] and oil recovery.[12] Most recently, they have even been used as a solvent for carrying out enzyme-based reactions.[14] Unfortunately, although supercritical fluids are being used effectively in a myriad of areas, we still lack a detailed understanding of the fundamental processes that govern these peculiar solvents.

In an effort to overcome this disparity, significant effort has been devoted to determining the fundamental aspects of solute–solute, solute–fluid, and solute–cosolvent interactions in supercritical fluids.[15-45] The bulk of these efforts have used optical

* Author to whom all correspondence should be addressed.

† Dedicated to Professor Gary M. Hieftje on the occasion of his 50th birthday.

(1) Reid, R. C.; Prausnitz, J. M.; Poling, B. E. *The Properties of Gases and Liquids*, 4th ed.; McGraw-Hill: New York, 1987.
(2) McHugh, M. A.; Krukonis, V. J. *Supercritical Fluid Extraction-Principles and Practice*; Butterworths: Boston, MA, 1986.
(3) Paulaitis, M. E.; Krukonis, V. J.; Kurnik, R. T.; Reid, R. C. *Rev. Chem. Eng.* **1983**, *1*, 179.
(4) Paulaitis, M. E.; Kander, R. G.; DiAndreth, J. R. *Ber. Bunsen-Ges. Phys. Chem.* **1984**, *88*, 869.
(5) Brennecke, J. F.; Eckert, C. A. *AIChE J.* **1989**, *35*, 1409.
(6) Klesper, E. *Angew. Chem., Int. Ed. Engl.* **1978**, *17*, 738.
(7) Novotny, M. V.; Springston, S. R.; Peaden, P. A.; Fjeldsted, J. C.; Lee, M. L. *Anal. Chem.* **1981**, *53*, 407A.
(8) *Supercritical Fluid Chromatography*; Smith, R. M., Ed.; Royal Society of Chemistry Monograph: London, UK, 1988.
(9) Smith, R. D.; Wright, B. W.; Yonker, C. R. *Anal. Chem.* **1988**, *60*, 1323A.
(10) Brunner, G. *Ion. Exch. Solvent Extr.* **1988**, *10*, 105.
(11) Eckert, C. A.; Van Alsten, J. G. *Environ. Sci. Technol.* **1986**, *20*, 319.
(12) *Supercritical Fluids - Chemical Engineering Principles and Applications*; Squires, T. G., Paulaitis, M. E., Eds.; ACS Symposium Series 329; American Chemical Society: Washington, DC, 1987.
(13) van Wasen, U.; Swaid, I.; Schneider, G. M. *Angew. Chem., Int. Ed. Engl.* **1980**, *19*, 575.
(14) Aaltonen, O.; Rantakyla, M. *CHEMTECH* **1991**, *21*, 240.
(15) Eckert, C. A.; Ziger, D. H.; Johnston, K. P.; Ellison, T. K. *Fluid Phase Equilib.* **1983**, *14*, 167.
(16) Eckert, C. A.; Ziger, D. H.; Johnston, K. P.; Kim, S. *J. Phys. Chem.* **1986**, *90*, 2738.
(17) Kim, S.; Johnston, K. P. *Ind. Eng. Chem. Res.* **1987**, *26*, 1206.

0002-7863/92/1514-5249$03.00/0

spectroscopy[17-34,43-45] as a tool to probe the aforementioned interactions. Many of these experimental studies have been advanced also by theoretical calculations and modeling.[35-42]

The general conclusions from these studies are the following: (1) that there is local density augmentation (i.e., solvent clustering or molecular charisma) about the solute near the critical point and (2) that density augmentation data can be interpreted using a simple expression derived from Kirkwood–Buff solution theory.[20] In addition, it has been suggested that there are enhanced solute–solute interactions near the critical point.[5,31,43-45] In fact, Combes et al.[43] recently reported density-dependent rates and product selectivities for cyclohexanone photodimerization in supercritical ethane and argued for solute–solute clustering.

The unique fluorescence characteristics of pyrene emission have been known for nearly 40 years.[46-54] In normal liquids, pyrene exhibits a structured violet emission, with the 0–0 transition occurring near 370 nm.[46] As the pyrene concentration is increased, the monomer fluorescence intensity eventually decreases, and a broad structureless aqua-blue emission appears at about 460 nm.[46-54] This emission band is due to a pyrene excimer, produced by the collisional association between an excited- and a ground-state pyrene molecule.[46-54] The absorbance spectral contours for dilute (monomer only) and concentrated (monomer + excimer) pyrene solutions are identical.[46] Furthermore, the emission-wavelength-dependent fluorescence excitation spectral contours are also identical.[54] This indicates that, in liquids, no ground-state dimerization occurs.

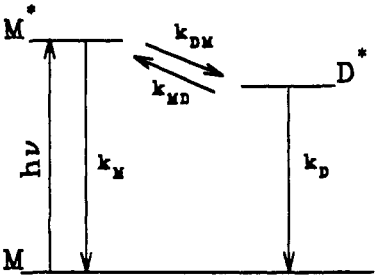

Figure 1. Energy-level diagram for pyrene excimer formation. Symbols represent the following: $h\nu$, absorbed photon; k_M, deexcitation rate from monomer species; k_{DM}, bimolecular rate coefficient for formation of the pyrene excimer; k_{MD}, unimolecular rate coefficient for dissociation of the pyrene excimer; and k_D, deexcitation rate from the excimer species. Note: no ground-state association is indicated.

The steady-state emission spectrum of monomeric pyrene has several characteristic vibrational peaks. The intensity of the 0–0 transition (I_1) is extremely solvent dependent[49-51] and increases with increasing solute–solvent interaction. In contrast, the 0–3 transition (I_3) is insensitive to solvent.[49-51] Thus, it is possible to probe solute–solvent interactions by following I_1/I_3; I_1/I_3 increases as solute–solvent interactions increase.[49-51] This ratio has been reported for pyrene in supercritical fluids[5,31,44,45] and is shown to increase with fluid density.

Brennecke et al.[5,31,44,45] have reported previously on pyrene fluorescence in supercritical CO_2, C_2H_4, and CF_3H. Steady-state emission spectra were used to show that there is density augmentation near the critical point.[45] Additional studies investigated the concentration dependence of the pyrene emission. The most intriguing aspect of these experimental results[5,31,44,45] is that an excimer-like emission was observed for pyrene concentrations in the low micromolar range. In normal liquids, pyrene forms an excimer that is generally observed at millimolar or higher pyrene concentrations.[46-54] Upon seeing this, Brennecke et al.[5,31,44,45] concluded that the excimer was a manifestation of increased solute–solute (pyrene–pyrene) interaction near the critical point of the fluid. Unfortunately, even though these steady-state experiments were well done, they suffer inherently from limited information content.[46-54] Specifically, on the basis of the steady-state emission data alone, one cannot determine the actual kinetics of the excimer-like process.[46-54] Furthermore, it is not[46-54] possible to distinguish between ground- and excited-state solute–solute interactions, if they exist.

In this paper, we report on the first complete steady-state and time-resolved fluorescence studies of pyrene emission in supercritical CO_2. Pyrene was chosen because it has been investigated previously[5,31,44,45] in supercritical fluids and the photophysics have been studied extensively in liquid solvents,[46-48] at interfaces,[52,53] and in organized media.[54] CO_2 was chosen because it is the most widely used supercritical fluid and accurate information exists on the density-dependent solubility of pyrene in CO_2.[55-57]

(18) Kim, S.; Johnston, K. P. *AIChE J.* **1987**, *33*, 1603.
(19) Brennecke, J. F.; Eckert, C. A. In *Proceedings of the International Symposium on Supercritical Fluids*, Nice, France; Perrut, M., Ed.; 1988; p. 263.
(20) Johnston, K. P.; Kim, S.; Combs, J. In *Supercritical Fluid Science and Technology*; Johnston, K. P., Penninger, J. M. L., Eds.; ACS Symposium Series; American Chemical Society: Washington, DC, 1989; Vol. 406, Chapter 5.
(21) Hyatt, J. A. *J. Org. Chem.* **1984**, *49*, 5097.
(22) Sigman, M. E.; Lindley, S. M.; Leffler, J. E. *J. Am. Chem. Soc.* **1985**, *107*, 1471.
(23) Sigman, M. E.; Leffler, J. E. *J. Phys. Chem.* **1986**, *90*, 6063.
(24) Yonker, C. R.; Frye, S. L.; Kalkwarf, D. R.; Smith, R. D. *J. Phys. Chem.* **1986**, *90*, 3022.
(25) Smith, R. D.; Frye, S. L.; Yonker, C. R.; Gale, R. W. J. *J. Phys. Chem.* **1987**, *91*, 3059.
(26) Yonker, C. R.; Smith, R. D. *J. Phys. Chem.* **1988**, *92*, 2374.
(27) Johnston, K. P.; Kim, S.; Wong, J. M. *Fluid Phase Equilib.* **1987**, *38*, 39.
(28) Yonker, C. R.; Smith, R. D. *J. Phys. Chem.* **1988**, *92*, 235.
(29) Okada, T.; Kobayashi, Y.; Yamasa, H.; Mataga, N. *Chem. Phys. Lett.* **1986**, *128*, 583.
(30) Kajimoto, O.; Futakami, M.; Kobayashi, T.; Yamasaki, K. *J. Phys. Chem.* **1988**, *92*, 1347.
(31) Brennecke, J. F.; Eckert, C. A. In *Supercritical Fluid Science and Technology*; Johnston, K. P., Penninger, J. M. L., Eds.; ACS Symposium Series; American Chemical Society: Washington, DC, 1988; Vol. 406, Chapter 2.
(32) Hrnjez, B. J.; Yazdi, P. T.; Fox, M. A.; Johnston, K. P. *J. Am. Chem. Soc.* **1989**, *111*, 1915.
(33) Betts, T. A.; Bright, F. V. *Appl. Spectrosc.* **1990**, *44*, 1196.
(34) Betts, T. A.; Bright, F. V. *Appl. Spectrosc.* **1990**, *44*, 1204.
(35) Debenedetti, P. G. *Chem. Eng. Sci.* **1987**, *42*, 2203.
(36) Debenedetti, P. G.; Kumar, S. K. *AIChE J.* **1988**, *34*, 645.
(37) Debenedetti, P. G.; Mohamed, R. S. *J. Chem. Phys.* **1989**, *90*, 4528.
(38) Cochran, H. D.; Lee, L. L.; Pfund, D. M. *Fluid Phase Equilib.* **1988**, *39*, 161.
(39) Shing, K. S.; Chung, S. T. *J. Phys. Chem.* **1987**, *91*, 1674.
(40) Gitterman, M.; Procaccia, I. *J. Chem. Phys.* **1983**, *78*, 2648.
(41) Cochran, H. D.; Pfund, D. M.; Lee, L. L. *Sep. Sci. Technol.* **1988**, *23*, 2031.
(42) Petsche, I. B.; Debenedetti, P. G. *J. Chem. Phys.* **1989**, *91*, 7075.
(43) Combes, J. R.; Johnston, K. P.; O'Shea, K. E.; Fox, M. A. In *Recent Advances in Supercritical Fluid Technology*; Bright, F. V., McNally, M. E., Eds.; ACS Symposium Series; American Chemical Society: Washington, DC, in press.
(44) Brennecke, J. F.; Tomasko, D. L.; Peshkin, J.; Eckert, C. A. *Ind. Eng. Chem. Res.* **1990**, *29*, 1682.
(45) Brennecke, J. F.; Tomasko, D. L.; Eckert, C. A. *J. Phys. Chem.* **1990**, *94*, 7692.
(46) Birks, J. B. *Photophysics of Aromatic Molecules*; Wiley-Interscience: New York, 1970.
(47) Förster, T. H.; Kasper, K. *Z. Phys. Chem.* **1954**, *1*, 275.
(48) Birks, J. B.; Dyson, D. J.; Munro, I. H. *Proc. Roy. Soc. A* **1963**, *275*, 575.
(49) Dong, D. C.; Winnik, M. A. *Can. J. Chem.* **1984**, *62*, 2560.
(50) Dong, D. C.; Winnik, M. A. *Photochem. Photobiol.* **1982**, *35*, 17.
(51) Ham, J. S. *J. Chem. Phys.* **1953**, *21*, 756.
(52) Lochmuller, C. H.; Wenzel, T. J. *J. Phys. Chem.* **1990**, *94*, 4230.
(53) Yamanaka, T.; Takahashi, T.; Kitamura, T.; Uchida, K. *Chem. Phys. Lett.* **1990**, *172*, 29.
(54) Yorozu, T.; Hoshino, M.; Imamura, M. *J. Phys. Chem.* **1982**, *86*, 4426.

Theory

In normal liquids, the kinetic model shown in Figure 1 describes the pyrene monomer and excimer emission process.[46] The species terms M, M*, and D* denote the ground-state monomer, excited-state monomer, and excited-state dimer (excimer), respectively. The terms k_M, k_D, k_{MD}, and k_{DM} represent the emissive rate coefficients for the monomer and excimer, the nonradiative unimolecular D* → M* + M (reverse) rate, and the nonradiative bimolecular M* + M → D* (forward) rate, respectively. The $h\nu$ symbolism denotes an absorption process that populates M* only; no D exists in the ground state.[46] The individual rate terms given in Figure 1 can be accurately recovered from a series of time-resolved fluorescence experiments.[46,48]

Briefly, adopting the symbolism developed by Birks et al.,[46,48] the intensity decay for the monomer ($i_M(t)$) and excimer ($i_D(t)$) are given by

$$i_M(t) = \frac{k_M[M^*]}{[M^*]_0} = \frac{k_M(\lambda_2 - X)}{\lambda_2 - \lambda_1}(e^{-\lambda_1 t} + Ae^{-\lambda_2 t}) \quad (1)$$

$$i_D(t) = \frac{k_D[D^*]}{[M^*]_0} = \frac{k_D k_{DM}[M]}{(\lambda_2 - \lambda_1)}(e^{-\lambda_1 t} - e^{-\lambda_2 t}) \quad (2)$$

In these expressions, $A = (X - \lambda_1)/(\lambda_2 - X)$, $\lambda_{1,2} = {}^1/_2[X + Y \pm \{(Y - X)^2 + 4k_{MD}k_{DM}[M] - XY\}^{1/2}]$, $X = k_M + k_{DM}[M]$, and $Y = k_D + k_{MD}$. The concentration terms [M*], [D*], and $[M^*]_0$ represent the concentrations of the monomer and dimer at any time t and the monomer at time $t = 0$, respectively. Inspection of eqs 1 and 2 shows that the intensity decays of the monomer and excimer are always described by a double exponential decay model with *apparent* emissive rates of λ_1 and λ_2.[46,48,58]

In order to obtain the k terms in Figure 1, one traditionally determined the apparent rates ($\lambda_{1,2}$) as a function of pyrene concentration.[46,48] That is, one evaluated the monomer and excimer decay traces *independently* over a broad pyrene concentration range ($\lambda_{1,2}$(pyrene)). These apparent rate terms were then plotted versus the pyrene concentration to yield estimates of the actual rate coefficients.[46,48] By increasing the range of pyrene concentrations studied, better estimates of the rates were obtained.[46,48]

In the present study, we recover all the rates in Figure 1 by simultaneous, global analysis of multiple fluorescence decay experiments.[59-64] That is, we analyze *simultaneously* the intensity decay traces from multiple wavelength and pyrene concentration experiments and recover the rate terms (Figure 1) directly. The advantages of this global approach are the following: (1) that one can use multiple experiments to help improve the accuracy of the recovered kinetic parameters and (2) that rate terms are recovered directly from the experimental data as opposed to being obtained from replotted individual results.[59-64] The goodness of fit between the experimental data and the assumed model are judged by the reduced χ^2, χ^2_r, residuals and the autocorrelation functions.[58] The theoretical treatment used to define the global algorithm can be found in ref 59.

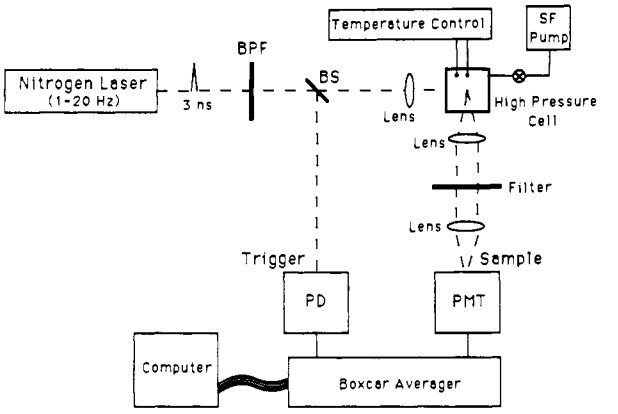

Figure 2. Schematic of the time-resolved fluorometer used for the study of pyrene in supercritical fluids. Abbreviations represent the following: BPF, bandpass filter; BS, beam splitter, PD, photodiode; and PMT, photomultiplier tube.

From the Einstein–Smoluchowski diffusion theory,[65,66] the bimolecular rate coefficient for a diffusion-controlled reaction is given by

$$k_{DM} = \frac{8000RT}{0.3\eta} \quad (3)$$

where R is the gas constant (J mol^{-1} K^{-1}), T is the temperature (K), and η is the fluid viscosity (P). For pyrene excimer emission in normal liquids, it has been found that the bimolecular rate (k_{DM}; M* + M → D*) generally follows this simple diffusion expression.[46,48]

Experimental Section

Instrumentation. A block diagram of the instrument constructed for the time-resolved fluorescence experiments is shown in Figure 2. A pulsed nitrogen laser (337 nm; LSI Inc., Model LS 337) is used as the excitation source. The laser output is passed through a broadband absorption filter centered at 340 nm (BPF) to eliminate extraneous plasma discharge. Typically, the laser is operated at a repetition rate of 10–15 Hz and the pulse duration is about 3 ns. A fraction of the laser beam is split off by a fused silica beam splitter (BS) and directed to a photodiode (PD). The current pulse from the photodiode serves as the electronic trigger for the boxcar averager. The laser beam is then focused with a fused silica lens (f = 150 mm) into the high-pressure optical cell.

The sample chamber comprises a light-tight aluminum housing and was constructed in house specifically for our high-pressure optical cells.[33] These optical cells are fabricated from 303 stainless steel.[33] The internal volume is about 5 mL, the cell body is water jacketed for temperature control, and there are four fused silica windows to allow optical access to the supercritical solvent.[33] The high-pressure window seals are maintained using a set of in-house-designed stainless steel–lead–brass compression seals. Initial designs used Viton O-ring seals, but a significant level of fluorescent impurity was continually extracted from the O-ring and contaminated the fluid sample. Attempts to alleviate this problem with Teflon seals solved the impurity problem; however, pyrene absorbed strongly into the Teflon O-rings. The metal-based seals solved both these problems.

Following excitation, the resulting fluorescence is collected by a fused silica lens (f = 50 mm) and collimated, filtered through an interference filter (10-nm bandpass), and focused with a second lens (f = 50 mm) onto the photocathode of a photomultiplier tube (PMT; Hamamatsu Model R372). The biasing potential (typically −650 V dc) for the PMT is supplied by a high-voltage power supply (SRS; Model PS 350). The PMT dynode circuitry is designed for fast response and is similar to systems described previously.[67,68]

The current pulse output from the PMT anode is amplified 5-fold (SRS; Model SR 445) and then directed to the input of a gated integrator/boxcar averager (SRS; Model SR 250). Data acquisition and control (RS-232) are carried out with an Epson Equity I+ personal

(55) Johnston, K. P.; Ziger, D. H.; Eckert, C. A. *Ind. Eng. Chem. Fundam.* **1982**, *21*, 191.
(56) Bartle, K. D.; Clifford, A. A.; Jafar, S. A. *J. Chem. Eng. Data* **1990**, *35*, 355.
(57) Mitra, S.; Wilson, N. K. *J. Chromatogr. Sci.* **1991**, *29*, 305.
(58) Demas, J. N. *Excited State Lifetime Measurements*; Academic Press: New York, 1983; Chapter 4.
(59) Beecham, J. M.; Gratton, E. In *Time-Resolved Laser Spectroscopy in Biochemistry*; Lakowicz, J. R., Ed.; SPIE: Bellingham, WA, 1988; Proc. SPIE 909, p 70.
(60) Beecham, J. M.; Ameloot, M.; Brand, L. *Chem. Phys. Lett.* **1985**, *120*, 466.
(61) Beecham, J. M.; Ameloot, M.; Brand, L. *Anal. Instrum.* (N.Y.) **1985**, *14*, 379.
(62) Huang, J.; Bright, F. V. *J. Phys. Chem.* **1990**, *94*, 8457.
(63) Ameloot, M.; Boens, N.; Andriessen, R.; Van den Bergh, V.; De Schryver, F. C. *J. Phys. Chem.* **1991**, *95*, 2041.
(64) Andriessen, R.; Boens, N.; Ameloot, M.; De Schryver, F. C. *J. Phys. Chem.* **1991**, *95*, 2047.
(65) Debye, P. *Trans. Electrochem. Soc.* **1942**, *82*, 205.
(66) Barrow, G. M. *Physical Chemistry*, 4th ed.; McGraw-Hill: New York, 1979; Chapter 19.
(67) Harris, J. M.; Lytle, F. E.; McCain, T. C. *Anal. Chem.* **1976**, *48*, 2095.
(68) Lytle, F. E. *Anal. Chem.* **1974**, *46*, 545A.

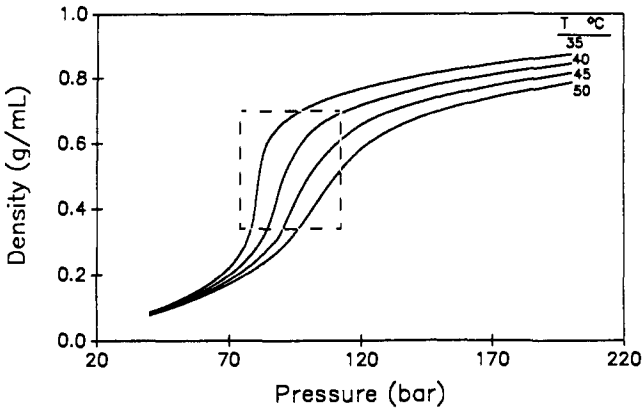

Figure 3. Isotherms for CO_2. The area contained within the box indicates the region over which experiments were carried out.

computer. The control/acquisition software was developed in our laboratory and is written in BASIC. Data analysis is performed off-line on a Tri-Star 486 33-MHz microcomputer.

All steady-state fluorescence experiments were carried out using a SLM 48000 MHF spectrofluorometer (SLM Instruments, Urbana, IL) modified to accommodate the high-pressure optical cells.[33,34] A 450-W Xe-arc lamp serves as the excitation source, and monochromators are used for excitation and emission wavelength selection.

The pressure within the optical cell is adjusted using a microprocessor-controlled supercritical fluid syringe pump (Isco; Model SFC-260D), and the pressure is monitored using a Heise gauge. The temperature of the cylinder head is regulated using a VWR 1140 temperature bath. The fluid flow into the pump is directed through a 2-μm fritted filter to minimize particulates. The pump output is directed through a series of valves into the optical high-pressure cell, which is temperature controlled (±0.1 °C) by a Lauda RLS-6 temperature bath.[33] The local temperature within the cell is determined using a thermocouple (Cole Palmer) placed directly into the cell body.

Sample Preparation. SFC grade CO_2 (<5 ppm O_2) was purchased from Scott, and pyrene (99%) was obtained from Aldrich. The pyrene purity was checked by reversed-phase HPLC (C_{18}), and all reagents were used as received. Stock solutions of pyrene were prepared in absolute ethanol (Quantum).

In order to prepare a sample for study, an aliquot of the stock pyrene solution (1 mM) is micropipetted directly into the optical cell, and the solvent is removed by placing the cell in a heated (60 °C) oven for several hours. After complete evaporation of the ethanol, the cell is connected to the high-pressure pump through a series of valves.[33] Residual O_2 is removed from the cell by maintaining a vacuum (50 μmHg) for 10–15 min. The cell vacuum is monitored using a vacuum gauge (Huntington, Model TGC-201).

To charge the cell, the pump head and optical cell are brought to the same temperature to minimize temperature gradients. The cell is pressurized to the desired pressure and allowed to equilibrate for about 30 min. When density studies are performed, the optical cell remains attached to the high-pressure pumping system, and the pressure is adjusted as required (low → high). In a given experiment, the molar concentration of pyrene remains constant. The density (ρ) and viscosity of CO_2 were obtained directly from the literature.[69,70]

Because supercritical fluids cluster most strongly in the highly compressible region about the critical point,[15-45] we investigated this region in detail (Figure 3).

Data Acquisition and Analysis. All experiments were conducted within the region indicated in Figure 3. All decay traces were collected in triplicate and averaged. The actual point-by-point uncertainties were then input into the global analysis scheme as weighting factors.[58,59] The gate width was 1.5 ns, and the scans were performed from t = 0 to 600 ns. More lengthy acquisitions to 1000 ns yielded statistically (95% confidence level) the same results as the shorter time scans. Three independent sets of experiments were performed to determine the imprecisions in the reported kinetic terms. All uncertainties and error bars are reported at ±1 standard deviation of the mean value.

The global analyis software (Globals Unlimited; Urbana, IL) was used to model the experimental data. In all cases, the simplest model that described the observed decay kinetics was given by Figure 1. Global χ^2_r were always in the range 0.9–1.15. In a typical analysis, decay traces acquired at three emission wavelengths (400, 450, and 480 nm) and two pyrene concentrations (75 and 100 μM) were analyzed (six total experiments) simultaneously and fit to an excited-state model, shown in Figure 1. Pyrene concentrations in excess of 100 μM were not used because of solubility problems[55-57] (vide infra). Concentrations below 70 μM were not used because minimal excimer is observed. The desired rate terms are recovered by nonlinear least squares.[58,59]

(69) Angus, A.; Armstrong, B.; de Reuck, K. M. *International Thermodynamic Tables of the Fluid State Carbon Dioxide*; Pergamon Press: New York, 1976.

(70) Golubev, I. F.; Petrov, V. A. *Tr. GIAP* **1953**, *2*, 5.

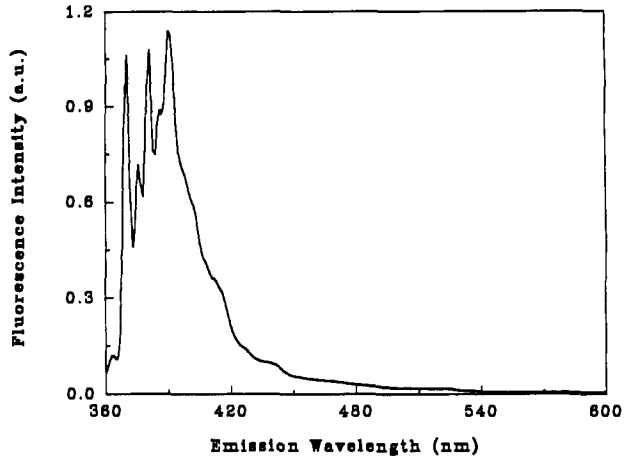

Figure 4. Steady-state fluorescence emission spectrum for 10 μM pryene in supercritical CO_2. T = 31.4 °C; P = 76 bar. λ_{ex} = 337 nm. Excitation spectral bandpass = 16 nm. Emission spectral bandpass = 2 nm.

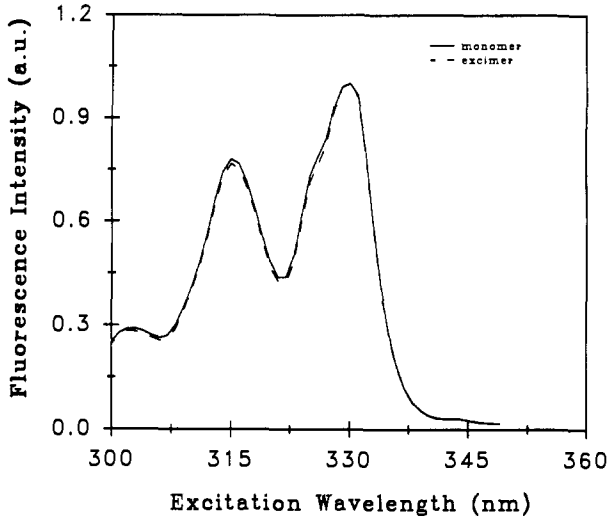

Figure 5. Normalized, emission-wavelength-dependent steady-state fluorescence excitation spectra for 10 μM pyrene in supercritical CO_2. T = 31.4 °C; P = 76 bar. λ_{em} = 380 nm for monomer. λ_{em} = 460 nm for excimer. Excitation spectral bandpass = 2 nm. Emission spectral bandpass = 16 nm.

Results and Discussion

Steady-State Experiments. Figure 4 shows a typical steady-state emission spectrum for 10 μM pyrene in CO_2 (T_c = 31 °C; P_c = 73.8 bar; ρ_c = 0.465 g/mL) at 31.4 °C and 76 bar. Similar spectral contours are seen at 31.4, 34.0, 37.7, and 46.0 °C over a reduced density ($\rho_r = \rho/\rho_c$) range of 0.70–1.6 (not shown). There are several interesting aspects of these results. First, the vibrational fine stucture of the pyrene emission is well preserved, and the I_1 and I_3 peaks are well resolved (vide infra). Second, there is no hint of any aqua-blue excimer-like emission.

Figure 5 shows a pair of normalized emission-wavelength-dependent steady-state excitation spectra for the sample shown in Figure 4. To acquire the "monomer" spectrum (—), the emission wavelength was adjusted to a region of the emission spectrum where monomer would predominate (380 nm), and then the excitation wavelength was scanned. The "excimer" spectrum (– – –) was obtained in a similar fashion, but the emission wavelength

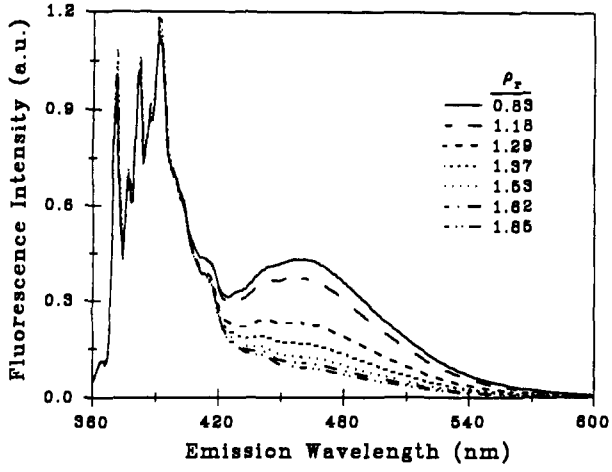

Figure 6. Steady-state emission spectra for 100 μM pyrene in sub- and supercritical CO_2 as a function of density. T = 31.4 °C. λ_{ex} = 337 nm. Excitation spectral bandpass = 16 nm. Emission spectral bandpass = 2 nm.

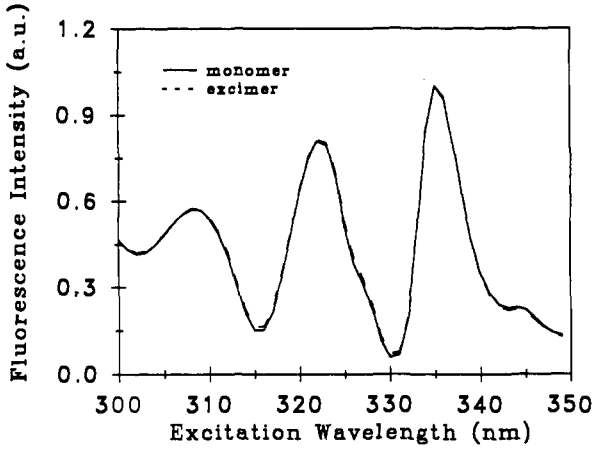

Figure 7. Normalized, emission-wavelength-dependent steady-state excitation spectra for 100 μM pyrene in supercritical CO_2. T = 34.1 °C; P = 79.4 bar. λ_{em} = 380 nm for monomer. λ_{em} = 460 nm for excimer. Excitation spectral bandpass = 2 nm. Emission spectral bandpass = 16 nm.

was adjusted to a region (460–480 nm) where, if it were to be present, the excimer-like emission would appear. The most interesting and important feature of these spectra is that they are essentially superimposable. These results were not unexpected and are consistent with ground-state homogeneity for dilute pyrene in CO_2. Again, fluid density and temperature had no effect on the excitation contours; they were always superimposable.

In contrast to the 10 μM pyrene results, Figure 6 shows a series of density-dependent emission spectra for 100 μM pyrene in supercritical CO_2 (T = 31.4 °C). Several aspects of these data merit further discussion. First, the excimer-like emission is clearly evident at about 460 nm. Second, in normal liquids, one would not observe any excimer at this pyrene concentration.[46] Third, the excimer-like emission is clearly density dependent; it decreases with higher fluid density. From this type of information alone Brennecke et al.[45] proposed that there was increased solute–solute interaction in supercritical fluids. That is, it was proposed that the pyrene species were somehow preferentially associating prior to being excited. This association was then proposed to result in the observance of excimer-like emission.[45] Unfortunately, on the basis of emission spectra alone one cannot absolutely rule out other mechanisms being manifest as the excimer-like emission.[46-54]

Figure 7 shows a pair of normalized, emission-wavelength-dependent steady-state excitation spectra for the sample shown in Figure 6. This set of spectra were obtained following the protocol outlined above for the more dilute 10 μM pyrene sample. Once again, the excitation contours are essentially superimposable,

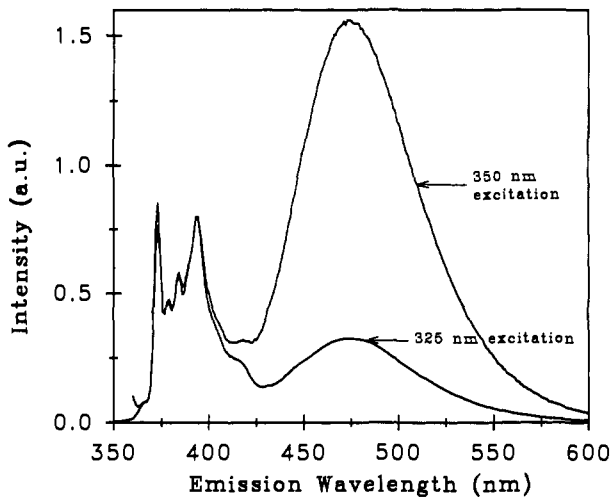

Figure 8. Excitation-wavelength-dependent steady-state emission spectra for 0.5 μM pyrene in γ-CD excited at 325 and 350 nm. The ground-state dimer is preferentially excited at 350 nm. Excitation spectral bandpass = 16 nm. Emission spectral bandpass = 2 nm.

and temperature and density have no effect on the contours (vide infra). These results are completely consistent with only a single species (individual pyrene molecules) existing in the ground state.[46-54]

At this point we questioned if our methodology was capable of detecting ground-state pyrene dimers. To this end, we investigated first pyrene complexed with γ-cyclodextrin (γ-CD).[54] Cyclodextrins are an interesting class of water-soluble macrocycles made up of between six and eight glucose monomers covalently linked to form a toroidally-shaped truncated cone.[71] The exterior of the cyclodextrin is hydrophilic, and the interior cavity is moderately hydrophobic. Thus, the cyclodextrin cavity can serve as a site in which to sequester (host) selectively an array of molecular species (guests). This host–guest association is generally governed by the size of the cavity and guest and the shape/charge of the guest. The pyrene–γ-CD complex is especially interesting because two pyrene species can coinclude within a single γ-CD cavity.[54] That is, one can form an appreciable amount of ground-state dimer within the γ-CD.[54] Moreover, this dimer can be formed when the total pyrene concentration is several orders of magnitude below that required for excimer emission (i.e., 10^{-7} M).[54]

Figure 8 shows a pair of excitation-wavelength-dependent emission spectra for 0.5 μM pyrene in 10 mM γ-CD. The most interesting aspect of these spectra is that the relative contribution from the excimer-like emission is strongly dependent on the excitation wavelength. For example, the relative amount of excimer-like emission increases several-fold when one varies the excitation wavelength from 325 to 350 nm. This result is consistent with two subpopulations existing in the ground state (monomer and dimer).[54] This conclusion is supported further by inspection of the normalized, emission-wavelength-dependent excitation spectra for this system (Figure 9).

In obvious contrast to the superimposable spectra seen for pyrene in supercritical CO_2 (Figure 7), we see here (Figure 9) significant differences in the spectra. Once again, this is completely consistent with there being more than one subpopulation in the ground state.[54] In addition, we can now see that by exciting at 350 nm we preferentially excite the ground-state pyrene dimer. Thus, we feel confident that if excimer-like dimers were to exist in the ground state, they would be detected as differences in the emission-wavelength-dependent excitation spectra (compare Figures 7 and 9). Of course, if the nature of the solute–solute interactions were such that they did not manifest themselves as a preformed (face-to-face) excimer-like dimer, we may not be able to detect or quantify such a solute–solute interaction.[72]

(71) Saenger, W. *Angew. Chem., Int. Ed. Engl.* **1980**, *19*, 344.

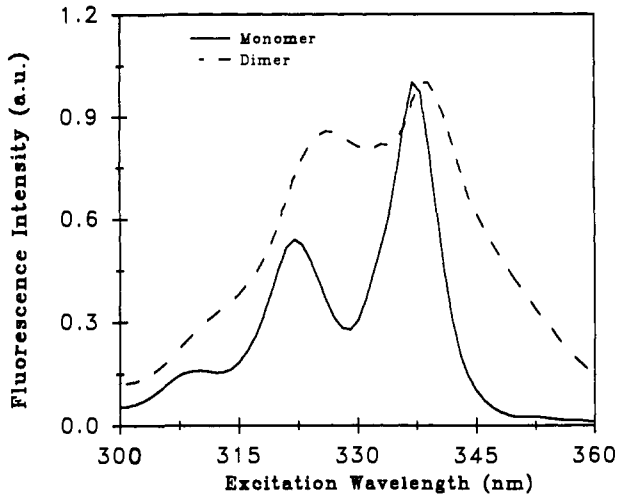

Figure 9. Normalized, emission-wavelength-dependent steady-state excitation spectra of 0.5 μM pyrene in γ-CD. λ_{em} = 380 nm for monomer. λ_{em} = 460 nm for excimer. Excitation spectral bandpass = 2 nm. Emission spectral bandpass = 16 nm.

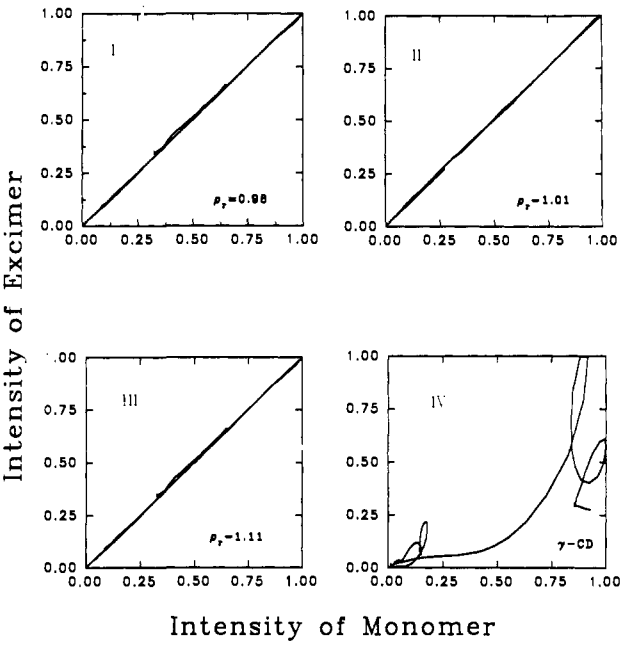

Figure 10. Correlation plots for pyrene in various media. Panels I–III: 100 μM pyrene in CO_2 as a function of fluid density at T = 34.1 °C. Panel IV: 0.5 μM pyrene in 10 mM γ-CD. See text for discussion.

A simple and effective means to compare a pair of emission-wavelength-dependent excitation spectra is to prepare an intensity–intensity correlation plot. In this approach, the excitation spectra are first normalized at the peak maxima, and then the intensity of the "excimer" scan (λ_{em} = 460 nm) is plotted versus the intensity of the "monomer" scan (λ_{em} = 380 nm). If the pyrene spectral contours overlap completely, for example, if there is no ground-state, dimer-like association, we would anticipate a straight line with a slope of unity, an intercept of 0, and a correlation coefficient of unity. Figure 10 shows a set of typical density-dependent correlation plots for 100 μM pyrene in supercritical

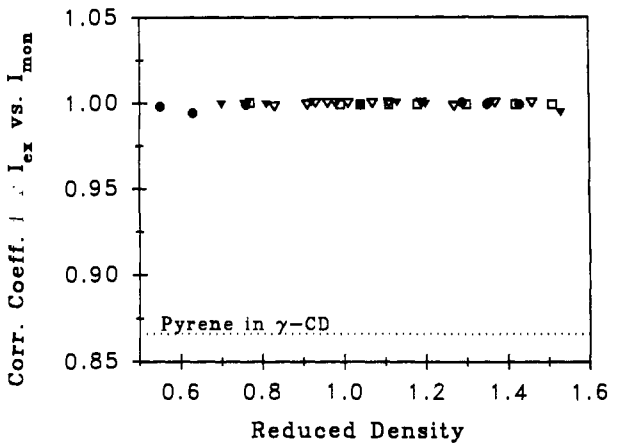

Figure 11. Recovered correlation coefficients for correlation plots (cf. panels I–III; Figure 10) as a function of fluid temperature and reduced density. Also shown is the correlation coefficient for pyrene in γ-CD (···; Figure 10; panel IV). Symbol, T_r: ●, 1.00; ▽, 1.01; ▼ 1.02; □, 1.03.

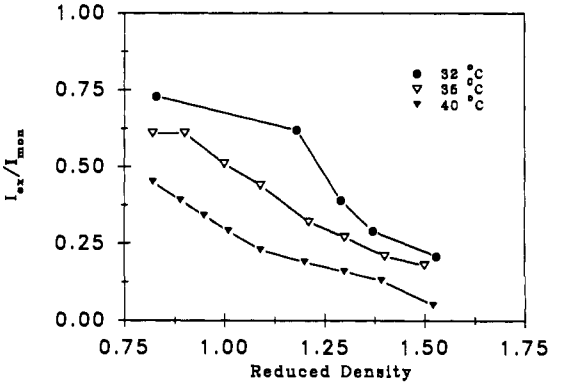

Figure 12. Relative amount of pyrene excimer as a function of fluid temperature and reduced density. The expression I_{ex}/I_{mon} is the ratio of excimer to monomer. The terms I_{ex} and I_{mon} denote the integrated areas between 440 and 500 nm and between 367 and 420 nm, respectively.

CO_2 (panels I–III). Similarly, panel IV shows results for 0.5 μM pyrene in 10 mM γ-CD. Clearly, the supercritical fluid data are completely consistent with there being no ground-state pyrene–pyrene association.[72] This result is in contrast with the correlation plot for pyrene–γ-CD (panel IV), which is completely nonlinear.

To ensure that these particular results are not anomalous we carried out an extensive series of experiments on 100 μM pyrene in subcritical and supercritical CO_2. The results are summarized in Figure 11, which shows the correlation coefficient (r^2) of the correlation plot (e.g., Figure 10) as a function of reduced density and temperature. These results are completely consistent with their being a single pyrene species in the ground state: individual pyrene monomers.

Although density does not affect ground-state pyrene (Figure 11), it does affect the relative amount of excimer-like emission (Figure 6). To illustrate this point more clearly, Figure 12 shows that fluid density and temperature each affect the relative amount of excimer formed. For example, when fluid density or temperature increases, the relative amount of excimer formed decreases. Unfortunately, it is not possible to explain these particular observations without knowledge of the kinetics of the excimer-like process.[48-54]

Time-Resolved Experiments. Time-resolved fluorescence spectroscopy provides a convenient means to access the kinetic parameters that describe the pyrene emission process.[48-54] However, before we begin exploring the kinetics it is important to review our understanding to this point and anticipate any potential problems. First, from our steady-state experiments there is no evidence for ground-state excimer-like (solute–solute) association in the pyrene–CO_2 system. This implies that we could potentially have a photophysical model given by Figure 1. Second,

(72) One may be inclined to believe that only the face-to-face species is quantifiable via our techniques. However, recent work (cf.: Winnik, F. M. *Macromolecules* **1990**, *23*, 233) with less structured polymer systems shows that ground-state association is also evident for pyrene. Again, it may be that the face-to-face ground-state dimer contributes, but the fact that one can observe a significant spectral shift when there is preassociation (prior to excitation) argues that we would have been able to see and quantify preferential solute–solute interactions using our techniques.

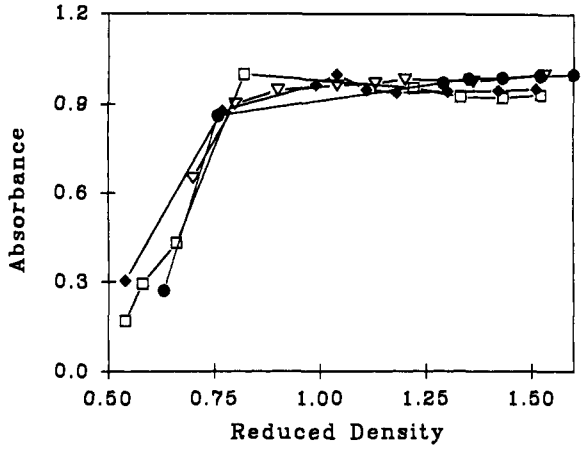

Figure 13. Steady-state absorbance (at 325 nm) for 100 μM pryene as a function of CO_2 reduced density. All pyrene is solubilized above a reduced density of 0.80. Symbol, T_r: ●, 1.00; ▽, 1.01; □, 1.03; ♦, 1.05.

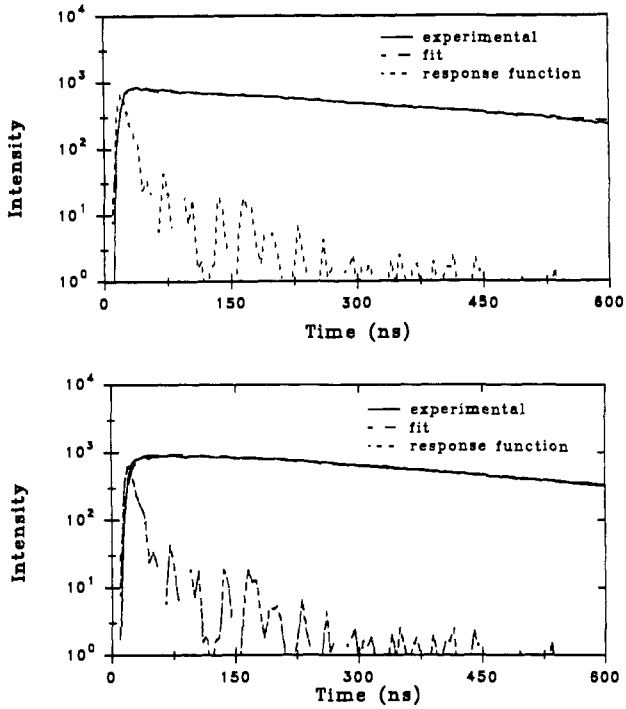

Figure 14. Typical time-resolved fluorescence decay traces for 100 μM pyrene in supercritical CO_2. T_r = 1.00; P_r = 1.02. Upper and lower panels represent monomer (400 nm) and excimer (480 nm) emission, respectively.

we must be concerned with the density-dependent solubility of pyrene in CO_2. This is important, because our fitting algorithm requires accurate knowledge of the analytical concentration of pyrene actually *dissolved* in the supercritical fluid. After performing a series of absorbance measurements (Figure 13), we determined that it was not possible to solubilize 100 μM pyrene below a reduced density of 0.8. Therefore, all time-resolved experiments were carried out at reduced densities greater than 0.8.

As discussed in the Theory section, one can use transient fluorescence experiments to determine the individual rate parameters of a given photophysical model. To this end, Figure 14 shows a pair of typical time-resolved fluorescence decay traces for 100 μM pyrene in supercritical CO_2 (T_r = 1.00; P_r = 1.02). Note that the y-scale is logarithmic. The upper and lower panels show results for selective observation of the monomer (400 ± 10 nm) and excimer (480 ± 10 nm) regions of the emission spectrum. Several interesting features are apparent from these traces. First, both decay processes are nonexponential. Second, the excimer emission (lower panel) has a significant contribution from a species

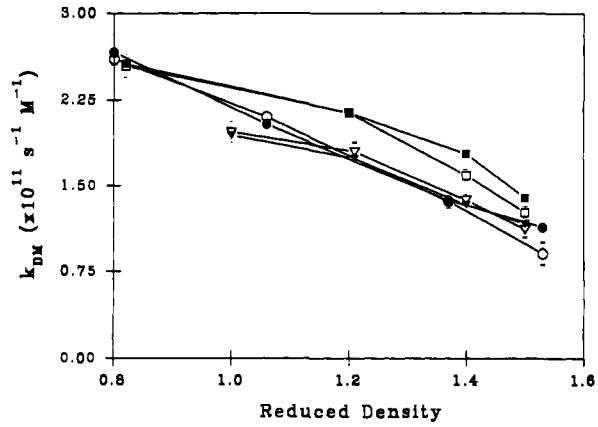

Figure 15. Recovered forward rates (k_{DM}) for pyrene excimer formation in CO_2 as a function of reduced density and temperature. The uncertainties represent ±1 standard deviation from the mean of three independent experiments. Filled symbols denote experimental results, and open symbols represent calculated values based on eq 3. Symbol, T_r: ●, 1.00; ▼, 1.01; ■, 1.03.

Table I. Experimentally Recovered and Theoretical Values for the Forward Bimolecular Rate Coefficient (k_{DM}) for Pyrene Excimer Formation in Supercritical CO_2

T (°C)	pressure (bar)	$k_{DM} \times 10^{11}$ (exptl) $(M^{-1}\ s^{-1})^a$	$k_{DM} \times 10^{11}$ (theor) $(M^{-1}\ s^{-1})^b$
32	75.0	2.61 ± 0.08	2.67
	75.5	2.10 ± 0.05	2.04
	79.3	1.36 ± 0.05	1.37
	89.6	0.90 ± 0.15	1.13
35	80.7	1.97 ± 0.12	1.94
	82.7	1.80 ± 0.08	1.74
	89.3	1.37 ± 0.07	1.33
	97.2	1.11 ± 0.05	1.16
40	86.2	2.55 ± 0.07	2.57
	93.8	2.14 ± 0.03	2.14
	103.4	1.59 ± 0.03	1.78
	116.9	1.26 ± 0.06	1.39

[a] Experiments were performed by maintaining the corresponding temperature and adjusting the pressure. Fluorescence decays were obtained at four different wavelengths for two different pyrene concentrations. The rate coefficients were recovered by linking the spectral parameters over the entire multidimensional data surface. [b] Calculated from the Smoluchowski equation (eq 3).

that "grows in" between 20 and 150 ns. This growing in is reflected by an upward curvature in the decay trace in the 150-ns region and is a manifestation of the excimer taking time to form following photoproduction of M* (i.e., k_{DM} in Figure 1). Third, the fits between the experimental data and the excimer model shown in Figure 1 are very good (χ^2_r = 1.06). Detailed analysis of the remaining data sets were also consistent with the simple excimer model (Figure 1).

Figure 15 shows the experimentally recovered (open points) bimolecular rate coefficients (k_{DM}; Figure 1) for pyrene excimer formation as a function of CO_2 density and temperature. Three independent sets of experiments were carried out to determine the uncertainty associated with each point. The solid symbols denote the theoretical rate coefficient calculated when a diffusion-controlled process was assumed (eq 3). The viscosities used in the equation were obtained by plotting those values found in literature[70] for a given temperature and pressure and interpolating for the corresponding experimental conditions. The agreement between the experimentally recovered and calculated rates is very good. This is reflected further in Table I, which compiles the experimental and theoretical forward rates. These results indicate the following: (1) that there is no significant deviation in the reaction rate near the critical point and (2) that the pyrene excimer formation process in supercritical CO_2 is completely diffusion controlled over the density range studied. Thus, although the solvent molecules are able to cluster about the pyrene solute,[5,15-45]

Table II. Experimental Values for the Reverse Unimolecular Rate Coefficient (k_{MD}) for the Dissociation of Pyrene Excimer in Supercritical CO_2

T (°C)	pressure (bar)	$k_{MD} \times 10^9$ (s^{-1})[a,b]	$k_M \times 10^6$ (s^{-1})[a,b]	$k_D \times 10^6$ (s^{-1})[a,b]
32	75.0	0.41	3.09	1.11
	75.5	0.54	2.99	1.11
	79.3	1.02	2.85	7.15
	89.6	1.47	2.81	6.03
35	80.7	0.97	2.60	8.87
	82.7	1.09	2.34	9.25
	89.3	1.52	2.00	9.97
	97.2	7.34	1.39	9.20
40	86.2	1.09	3.53	9.90
	93.8	1.78	3.31	9.20
	103.4	1.96	3.05	9.52
	116.9	8.05	2.61	8.87

[a] Same experimental procedure as described in Table I. [b] Uncertainties in recovered rates ≤10%.

they are apparently not affecting directly the rate of excimer formation, or the association may not be stable or rigid. That is, the cluster "strength" is simply not great enough to offset the repulsive forces[48] between ground-state pyrene species. Of course, the major difference between the rates of excimer formation in liquids and supercritical fluids lie in their magnitude. For the supercritical fluid, the bimolecular rate coefficients are 2 orders of magnitude greater compared to those for pyrene in cyclohexane.[46,48] This is simply a result of the viscosity of supercritical CO_2 being essentially 2 orders of magnitude less than that for a liquid.[1-13]

Table II gives the rate coefficients for excimer dissociation (k_{MD}) and the emissive rates for the monomer (k_M) and the excimer (k_D) as a function of fluid density and temperature. The rate for excimer dissociation is 2 orders of magnitude faster in CO_2 than what has been reported in liquids.[48] However, recall that the forward rate is also 2 orders of magnitude faster due to lower viscosity and higher diffusivity. Therefore, the excited-state equilibrium constant (k_{DM}/k_{MD}) for pyrene excimer formation is the same order of magnitude in supercritical CO_2 and liquid cyclohexane.[48] This indicates that supercritical CO_2 does not affect the equilibrium of the pyrene excimer formation $\rightleftarrows$ dissociation.

Also shown in Table II are the values for the fluorescence decay of the monomer, k_M. This rate is the same as that reported by Birks et al.[48] and is minimally affected by temperature and CO_2 pressure. Again, it appears that supercritical CO_2 does not affect the photophysics of the pyrene monomer differently than what has been reported in liquids.

The rate term that is affected by supercritical CO_2 is that of the excimer. This rate is 2 orders of magnitude smaller than reported in liquids[48] and is slowest for temperatures and pressures nearest the critical point. Apparently, near the critical point the fluid is able to protect the excimer from nonradiative deactivation and allows it to remain in the excited state for a longer period of time. This result could be simply a consequence of the decreased interactions with the fluid or of the cluster being able to form about the excimer. If a cluster were to form about the excimer, it would make the local environment slightly more rigid and shield the excimer from quenchers (e.g., O_2).

To further investigate the effect of supercritical CO_2 on pyrene excimer formation, the energy of activation, E_a, and the Arrhenius frequency factor, A, have been evaluated as a function of reduced density. The values are collected in Table III. Interestingly, as we increase the fluid density, we see that the energy barrier height decreases. This indicates that the excimer formation reaction becomes more favorable. In contrast, our steady-state results show clearly that the fraction of excimer emission decreases with density. This result is explained by the significant decrease in the frequency factor. Thus, although the energy barrier height decreases at higher density, the frequency of encounters decreases such that the overall excimer reaction tends to decrease.

Table III. Recovered Activation Energy (E_a) and Arrhenius Frequency Factor (A) for Pyrene Excimer Formation in Supercritical CO_2 at various CO_2 Reduced Densities (ρ_r)[a]

ρ_r	E_a (kJ/mol)	A (s^{-1})
0.9	27.7	9.4×10^{15}
1.1	21.6	8.3×10^{14}
1.4	11.4	1.2×10^{13}
1.5	14.9	3.9×10^{13}

[a] Uncertainties in the recovered E_a and A terms ≤15%.

Conclusions

There has been much discussion of late on how supercritical solvents may affect chemical reactions. For example, pyrene excimer emission is observed in supercritical CO_2 at concentrations well below those required in normal liquids.[5,31,44,45] Thus, it is clear that some feature or features of supercritical CO_2 facilitate pyrene excimer formation. However, the fact that one sees excimer-like emission in supercritical solvents is only part of the story. The key issue is, *why* do pyrene excimers form in supercritical CO_2? The results from this work provide the first detailed insights into the kinetics of excimer formation in supercritical solvents and the effect of fluid density on this reaction.

From this work we see no evidence for the formation of ground-state, excimer-like pyrene dimers in supercritical CO_2. Thus, it does not appear that fluid clustering brings together pyrene species to preassociate prior to excitation.[73] This is not totally unexpected considering the well-known repulsive nature of ground-state pyrene species in liquid solvents.[46,48] Thus, although CO_2 clusters about the pyrene,[5,31,44,45] the strength of this association is not enough to overcome the overwhelming repulsive nature of ground-state pyrene molecules. Of course, these facts alone do not preclude the possibility that other forms of disordered ground-state associations exist (vide infra).

The combined steady-state and time-resolved experiments indicate that the formation of pyrene excimers in supercritical CO_2 is completely diffusion controlled and occurs only in the excited state. Thus, although the steady-state results could potentially be explained away by some form of spectroscopically nonobservable preassociation between pyrene molecules, one would be hard pressed to explain why the rate of excimer formation (k_{DM}) is not affected beyond that expected from diffusion control. For example, if one were to have a subpopulation of pyrene species that were, on average, preassociated in the ground state, one would expect k_{DM} to increase beyond that expected by diffusion control. In effect, the reacting partners would be placed in closer average proximity to one another and should react with each other more quickly. Similarly, one could have the case in which the fluid is so strongly clustered about the solute that the reaction is affected by diffusion (a more slowly diffusing pyrene-cluster species) or the pyrene species are shielded from one another by the cluster sheath. In either case, one would expect to see k_{DM} decrease compared to diffusion control. The experimental results are again inconsistent with all these schemes; the reaction is completely diffusion controlled over the density range studied.

After detailed analysis of the experimental data, we find that the reason for the observance of pyrene excimer in supercritical CO_2, at pyrene concentrations far below those required for similar observations in liquids, is a consequence of the following: (1) the decreased fluid viscosity (increased diffusivity) and (2) fluid–excimer interactions where CO_2 acts to stabilize the excimer excited state. Thus, CO_2 clustering does not influence how the excimer forms; it influences the excimer only after it forms.

Finally, we find that the amount of excimer decreases as CO_2 density increases. These density-dependent results are a consequence of the following: (1) the forward rate (k_{DM}) decreasing, (2) the reverse rate (k_{MD}) and excimer emissive rate (k_D) increasing, (3) the energy barrier heights decreasing slightly, and

(73) By this statement we are not implying that solute–solute interactions (in the most liberal of senses) do not occur. Clearly, the pyrene solutes interact with one another to form the excimer. The point of this statement is that CO_2 clustering does not affect how pyrene species are associated prior to excitation.

(4) the collisional frequency factor, between pyrene molecules, decreasing significantly with increasing density.

Currently, we are investigating the pyrene system in supercritical CF_3H and C_2H_4. We shall report the results of these efforts in due time.

Acknowledgment. This work has been supported generously by the United States Department of Energy (DE-FGO2-90ER14143). Special thanks are also extended to Kevin S. Litwiler for helping with the development of the time-domain acquisition software. We also thank Gary Sagerman for his continued help with instrument construction and Robert A. Osteryoung for use of his computer for data analysis. Finally, we appreciate the viscosity tables sent to us by David L. Tomasko.

Registry No. CO_2, 124-38-9; pyrene, 129-00-0.

Negative Ion Photoelectron Spectroscopy of Coordinatively Unsaturated Group VI Metal Carbonyls: $Cr(CO)_3$, $Mo(CO)_3$, and $W(CO)_3$

Ashfaq A. Bengali, Sean M. Casey, Chun-Lin Cheng, Jonathan P. Dick, P. Thomas Fenn, Peter W. Villalta, and Doreen G. Leopold*,†

Contribution from the Department of Chemistry, University of Minnesota, Minneapolis, Minnesota 55455. *Received November 12, 1991*

Abstract: Photoelectron spectra are reported for $Cr(CO)_3^-$, $Mo(CO)_3^-$, and $W(CO)_3^-$ anions prepared from the corresponding metal hexacarbonyls in a flowing afterglow ion source. The 488-nm spectra were obtained at an electron kinetic energy resolution of 5 meV using a new apparatus with improved mass resolution, which is described in this report. The spectra exhibit transitions between the ground electronic states of the anions and the neutral molecules, and they show weak activity in the symmetric CO stretching, MC stretching, MCO bending, and CMC bending vibrational modes. The observed vibrational structure indicates that the anions, like the neutral molecules, have C_{3v} equilibrium geometries. Principal force constants estimated from the measured vibrational frequencies of the neutral molecules are consistent with stronger metal–ligand bonding in the coordinatively unsaturated tricarbonyls than in the corresponding hexacarbonyl complexes. Franck–Condon analyses of the spectra indicate only small differences between the equilibrium bond lengths and bond angles of the anions and the corresponding neutral molecules. Electron affinities of 1.349 ± 0.006 eV for $Cr(CO)_3$, 1.337 ± 0.006 eV for $Mo(CO)_3$, and 1.859 ± 0.006 eV for $W(CO)_3$ are obtained. The electron affinity pattern observed among the three group VI metal tricarbonyls is compared with characteristic trends within triads of transition metal atoms and within the coinage metal dimer series. This comparison, combined with the results of previously reported theoretical calculations, suggests that the extra electron in the $M(CO)_3^-$ anions occupies an sp hybrid orbital. Related studies of the atomic anions yield improved values for the electron affinities of Cr (0.675 ± 0.004 eV), Mo (0.747 ± 0.004 eV), and W (0.817 ± 0.004 eV).

I. Introduction

Coordinatively unsaturated metal carbonyls are of interest as active species in catalytic reactions,[1-4] as the building blocks of stable organometallic complexes,[5] and as computationally tractable benchmarks against which to test theoretical models of metal–carbonyl bonding.[6] Although unsaturated metal carbonyls have many features in common with their fully ligated counterparts, qualitative differences in their electronic structure and bonding are also expected. As the ligands are sequentially removed from a coordinatively saturated $M(CO)_n$ complex, the metal atom will return from its low-spin s^0d^m valence electron configuration in the complex to its ground-state configuration, which in general is high-spin s^2d^{m-2} or s^1d^{m-1}. These electronic structure changes can be accompanied by dramatic variations in chemical reactivity, metal–ligand bond strengths, and molecular structure. For example, among the neutral $Fe(CO)_n$ molecules, sequential metal–ligand bond strengths differ by an order of magnitude,[7,8] and reactivity toward CO varies by almost 3 orders of magnitude.[9,10] Theoretical studies[11,12] indicate that the bonding in some metal–carbonyl fragments deviates significantly from the traditional model, in which the metal–carbonyl bond is viewed as arising from ligand-to-metal σ donation and metal-to-ligand π back-donation.

We report here a study of gas-phase $Cr(CO)_3$, $Mo(CO)_3$, and $W(CO)_3$ and the corresponding anions by negative ion photoelectron spectroscopy. These systems provide an opportunity to compare the bonding for open d-shell metal carbonyls of the first, second, and third transition series at a degree of coordinative

† Presidential Young Investigator, 1988–1993.

(1) Cotton, F. A.; Wilkinson, G. *Advanced Inorganic Chemistry*; Wiley: New York, 1988. Collman, J. P.; Hegedus, L. S.; Norton, J. R.; Finke, R. G. *Principles and Applications of Organotransition Metal Chemistry*; University Science Books: Mill Valley, CA, 1987.

(2) Iwasawa, Y., Ed. *Tailored Metal Catalysts*; D. Reidel: Dordrecht, The Netherlands, 1986. Bailey, D. C.; Langer, S. H. *Chem. Rev.* **1981**, *81*, 109–148.

(3) Ugo, R., Ed. *Aspects of Homogeneous Catalysis*; D. Reidel: Dordrecht, The Netherlands, 1984; Vol. 5. Parshall, G. W. *Homogeneous Catalysis*; Wiley: New York, 1980.

(4) Geoffroy, G. L.; Wrighton, M. S. *Organometallic Photochemistry*; Academic Press: New York, 1979.

(5) Hoffmann, R. *Angew. Chem., Intl. Ed. Engl.* **1982**, *21*, 711–724.

(6) Veillard, A. *Chem. Rev.* **1991**, *91*, 743–766.

(7) Engelking, P. C.; Lineberger, W. C. *J. Am. Chem. Soc.* **1979**, *101*, 5569–5573.

(8) Sunderlin, L. S.; Wang, D.; Squires, R. R. *J. Am. Chem. Soc.* **1992**, *114*, 2788–2796.

(9) Ouderkirk, A.; Weitz, E. *J. Chem. Phys.* **1983**, *79*, 1089–1091. Seder, T. A.; Ouderkirk, A. J.; Weitz, E. *J. Chem. Phys.* **1986**, *85*, 1977–1986.

(10) Weitz, E. *J. Phys. Chem.* **1987**, *91*, 3945–3953.

(11) (a) Barnes, L. A.; Rosi, M.; Bauschlicher, C. W., Jr. *J. Chem. Phys.* **1990**, *93*, 609–624. (b) Blomberg, M.; Brandemark, U.; Johansson, J.; Siegbahn, P.; Wennerberg, J. *J. Chem. Phys.* **1988**, *88*, 4324–4333. (c) Bauschlicher, C. W., Jr.; Bagus, P. S.; Nelin, C. J.; Roos, B. O. *J. Chem. Phys.* **1986**, *85*, 354–364. (d) Bauschlicher, C. W., Jr. *J. Chem. Phys.* **1986**, *84*, 260–267. (e) Bauschlicher, C. W., Jr.; Bagus, P. S. *J. Chem. Phys.* **1984**, *81*, 5889–5898. (f) Bagus, P. S.; Nelin, C. J.; Bauschlicher, C. W., Jr. *J. Vac. Sci. Technol.* **1984**, *A2*, 905–909.

0002-7863/92/1514-5257$03.00/0